Journal of Hydrology 645 (2024) 132262

Contents lists available at ScienceDirect

Journal of Hydrology

journal homepage: www.elsevier.com/locate/jhydrol

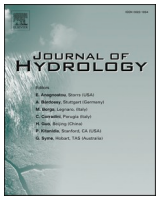

Exploring the compound nature of coastal flooding by tropical cyclones: A machine learning framework

Mario Di Bacco [a], Alessandro Contento [b], Anna Rita Scorzini [c,*]

[a] Department of Civil and Environmental Engineering, University of Florence, Firenze 50139, Italy
[b] College of Civil Engineering, Fuzhou University, Fujian 350108, China
[c] Department of Civil, Environmental and Architectural Engineering, University of L'Aquila, L'Aquila 67100, Italy

ARTICLE INFO

This manuscript was handled by Zhenxing Zhang, Editor-in-Chief, with the assistance of Zhenxing Zhang, Associate Editor

Keywords:
Compound flooding
Tropical cyclone
Data-driven model
Feature importance
Hurricane Harvey

ABSTRACT

Modeling inundation patterns resulting from compound flooding induced by tropical cyclones presents significant challenges due to the complex interplay of drivers and features affecting inundation mechanisms. This study introduces a machine learning framework designed to optimize the prediction of inundation depth by balancing model performance, computational costs and efforts for input data retrieval. Starting from a comprehensive, physics-informed identification of the potential explanatory variables, including features that capture local flood dynamics, as well as topological and geographical characteristics, the proposed methodology leverages a feature selection process based on permutation importance, which emphasizes the reduction in the number of inputs to streamline the modeling process without compromising accuracy. The framework has been tested using Hurricane Harvey as a case study. The analysis revealed performance in inundation depth prediction comparable to that of traditional hydrodynamic models available in the literature. Results demonstrated that focusing on the most informative features improves both model performance and efficiency, thus highlighting the need for careful feature selection for region-specific implementation of data-driven approaches for inundation depth prediction.

1. Introduction

Compound flooding induced by tropical cyclones is increasing worldwide against the backdrop of a changing climate, making low-lying coastal areas particularly vulnerable to these extreme events (Wahl et al., 2015; Zscheischler et al., 2018; Moftakhari et al., 2019). Projections of future sea level rise and changes in tropical cyclone climatology further exacerbate these risks (Zscheischler et al., 2018; Bevacqua et al., 2019; Marsooli et al., 2019; Camargo and Wing, 2021; IPCC, 2023), highlighting the urgent need for enhanced knowledge and advanced modeling tools for effective prediction and management.

Compound flooding arises when heavy rainfall, high river flow and extreme storm surge combine or occur in rapid succession (Ghanbari et al., 2021; Gori and Lin, 2022; Xu et al., 2023). Due to their nature, these hydrological and meteorological drivers may result in a synergistic effect, which exacerbate flooding risk and result in more severe consequences compared to those caused by isolated occurrences of the individual components (Bilskie and Hagen, 2018; Zscheischler et al., 2018; Huang et al., 2021; Gao et al., 2023; Lee et al., 2023; Tanim et al., 2024).

Traditionally, numerical models have been instrumental in forecasting flood events and assessing associated risks. Nonetheless, the compound effects of storm surge and riverine flows have mostly been analyzed by simulating these processes independently, failing to fully capture the complex dynamics of compound flooding events (Resio and Westerink, 2008; Santiago-Collazo et al., 2019; Wing et al. 2019; Gori et al., 2020; Moftakhari et al., 2019; Abbaszadeh et al., 2022; Zhong et al., 2024). For instance, even though detailed storm surge, hydrologic, and hydraulic models have been extensively developed and utilized, an oversimplified integration of model components describing the physical processes in coastal and inland areas may result in under- or over-estimation of both the extent and magnitude of inundation (Resio and Westerink, 2008; Wahl et al., 2015; Bilskie and Hagen, 2018; Santiago-Collazo et al., 2019; Abbaszadeh et al., 2022).

Hence, recognizing the interdependence of the processes involved, it is key to construct comprehensive compound flood models that seamlessly integrate coastal and inland inundation mechanisms (Huang et al., 2021; Abbaszadeh et al., 2022). In recent years, research efforts have increasingly centered around the integration of coastal and

* Corresponding author.
E-mail addresses: mario.dibacco@unifi.it (M. Di Bacco), alessandro@fzu.edu.cn (A. Contento), annarita.scorzini@univaq.it (A.R. Scorzini).

https://doi.org/10.1016/j.jhydrol.2024.132262
Received 21 July 2024; Received in revised form 25 September 2024; Accepted 10 October 2024
Available online 29 October 2024

hydrological-hydrodynamic models to address the complexity of compound floods (Saksena et al., 2020; Tanim and Goharian, 2021; Xu et al., 2023). Current approaches for integrating two or more numerical models can be categorized based on the technique used to transfer or exchange information between each component simulating the individual physical process involved: (i) one-way coupling, where the output from one model serves as the input for another; (ii) loose coupling, which consists in models running independently and concurrently, while information is reciprocally exchanged in an iterative manner; (iii) tightly coupling, which involves an exchange of information between different models within the same computational framework and (iv) full coupling, where the governing equations of all the relevant physical processes are solved simultaneously within an integrated modeling framework. Despite the practical advantages of loose coupling, an accurate prediction of compound flooding would require the adoption of more comprehensive fully coupled modeling schemes that integrate coastal and fluvial drivers (Santiago-Collazo et al., 2019; Loveland et al., 2021; Xu et al., 2023). However, as the complexity of models increases, there is a notable rise in the computational resources required, especially when considering larger spatial and temporal scales, as well as finer resolutions. Consequently, it becomes essential to find a balance between accuracy, computational burden, and efficiency for flood inundation modeling, especially when used at large-spatial scales or for early-warning purposes.

In this context, the utilization of machine learning (ML) offers a promising approach for advancing understanding on the complex interplay of factors contributing to compound flooding, thereby providing insights into the key drivers and interactions governing these phenomena. Additionally, unlike conventional modeling approaches, which rely on mathematical approximations of the studied phenomena, ML algorithms autonomously discern patterns and relationships within data. They can identify nonlinearities and emergent behaviors inherent in compound flooding processes, potentially offering an alternative modeling approach for such inundation events. However, it is important to recognize that ML approaches demand significant amounts of high-quality data for effective model development. This requirement extends beyond mere data volume to include the comprehensiveness of the considered predictive features. For instance, besides information on the desired response variable (e.g., observed inundation depth in historical or synthetic events), careful data selection and retrieval on the possible features influencing the inundation mechanisms are necessary for an accurate representation of compound flooding phenomena (e.g., hazard information, such as storm surge and river stages, morphological and land-use features of the built and natural environment in the examined area).

While ML approaches have recently garnered increasing attention for modeling riverine inundation (Dikshit et al., 2021; Bentivoglio et al., 2022; Karim et al., 2023), their application to the more complex scenarios of compound flooding, especially from tropical cyclones, remains limited (Zahura and Goodall, 2022; Moradian et al., 2024).

In this context, the present paper proposes a comprehensive ML framework designed to analyze compound flooding and assess the dominant drivers controlling inundation depth in such events, by leveraging a feature selection process based on permutation importance. By pinpointing the key features for an efficient and effective data-driven modeling, this framework aims to enhance understanding of complex compound flooding events. The study utilizes Hurricane Harvey as a well-documented and representative case study of compound flooding in coastal regions (Blake and Zelinsky, 2018), capitalizing on the abundance of observed data available for this particular event. However, the framework is flexible and can be tailored for application in various geographical contexts susceptible to tropical cyclones, allowing for adaptability and replications across different regions.

The paper is structured according to the logical framework outlined above and illustrated in Fig. 1, which serves as a summarizing tool of the implemented procedure. Section 2 introduces the theoretical foundation for a data-driven approach aimed at inundation depth estimation for compound flooding induced by tropical cyclones. It begins with a physics-informed identification of point-based and areal features that serve as descriptors of the drivers influencing compound flooding mechanisms (Section 2.1). The section then demonstrates how these data can be used in a ML approach to develop predictive models and to gain insights into the contribution of the different drivers to the physics of the problem. The methodology is first presented in general terms (Section 2.2) and then applied to the specific case of Hurricane Harvey as an illustrative example (Section 3). Section 4 presents and discusses the results of the approach for the considered case, with a focus on the contribution of different features to the model's response. This leads to the derivation of conclusions in Section 5, emphasizing lessons learned from the study from a modeling perspective.

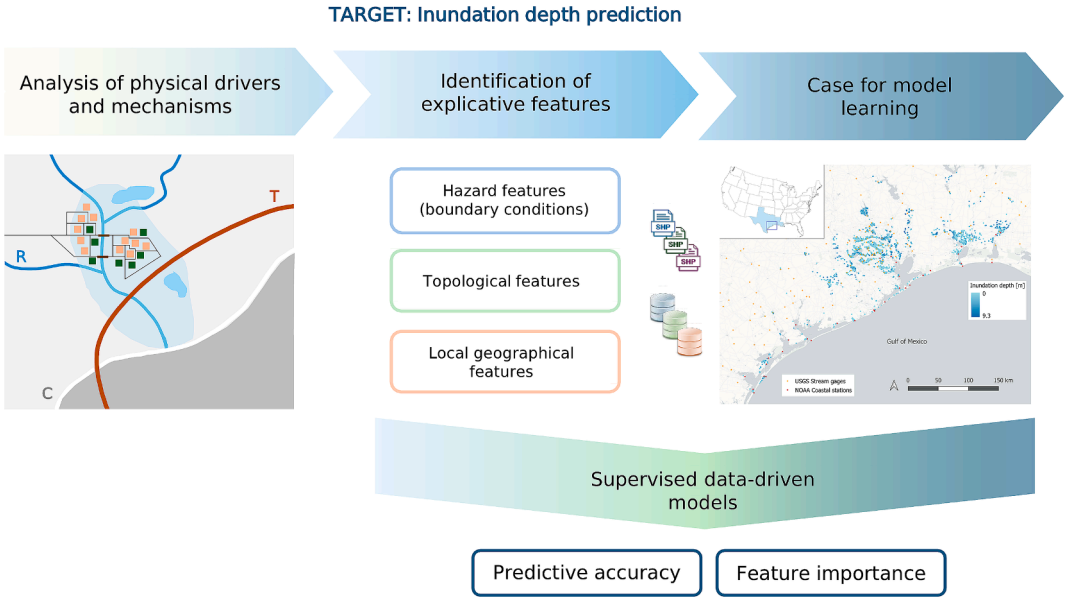

Fig. 1. Overview of the methodological framework.

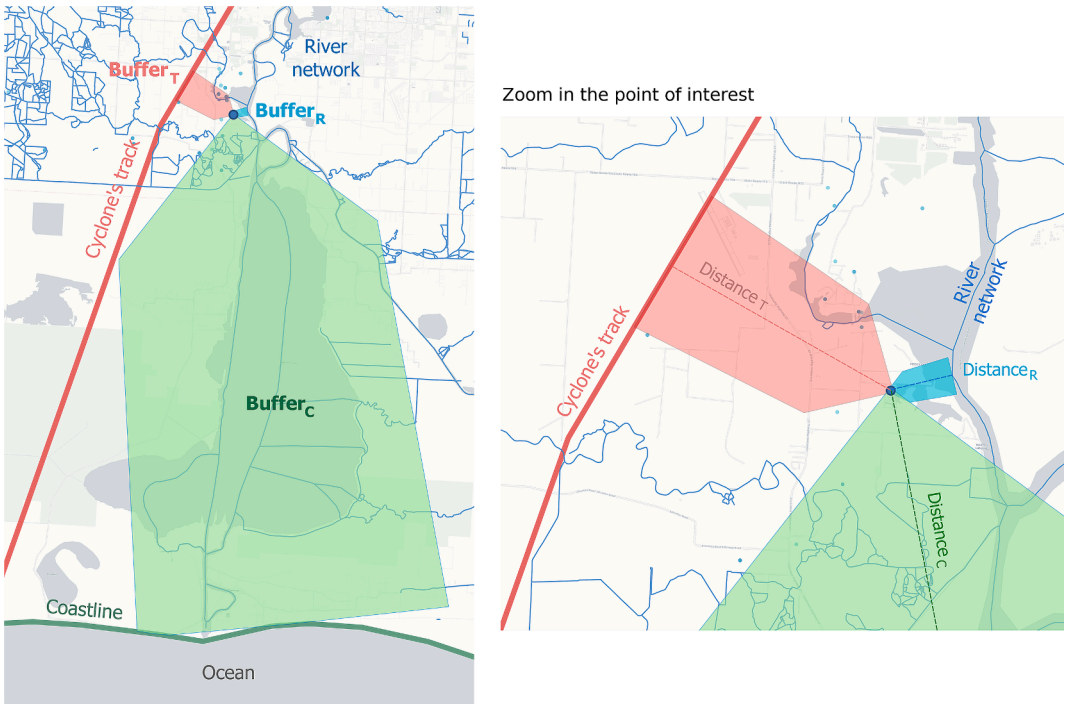

Fig. 2. Schematization of buffer geometries (in the coastal (C), river (R) and track (T) directions) for calculating proxy features for distributed local geographical features.

2. Data and methods

2.1. Framework for a data-driven approach for inundation depth assessment in compound flooding events

To develop a data-driven approach for assessing inundation depth induced by tropical cyclones, the initial step involves the identification of the relevant drivers for the problem at hand. A physics-informed approach can be adopted for this purpose, entailing in the identification of all possible drivers contributing to the inundation pattern in a coastal area affected by a tropical cyclone. The primary information, given the nature of compound events (Resio and Westerink, 2008; Moftakhari et al., 2019; Mitu et al., 2023), is represented by surge height measured along the coast and by water level at inland watercourses, which effectively serve as boundary conditions for the problem and inherently capture information on cyclone and hydrological variables, thus eliminating the need for additional data collection on hazard intensity. In the process of developing a predictive model, such information can derive from real-time storm surge and river stage forecasts in relevant stations, which can be respectively obtained using storm surge and rainfall-runoff models that are largely available in the literature (e.g., Dietrich et al., 2011; Beven, 2012; Lin et al., 2012; Kohno et al., 2018; Peel and McMahon, 2020). In addition to water levels along the coast and in watercourses, several other factors potentially contribute to flood propagation and, subsequently, to inundation severity in inland areas. A critical feature is the proximity to the boundary conditions (Brody et al., 2018; Darabi et al., 2019), such as the distance of a specific location of interest from the coast and from the hydrographic network (including rivers, streams or channels), with areas closer to them being more prone to flooding from rising water. As the straight-line distance between the point of interest (POI, hereinafter) for the prediction and the coastline or rivers increases, there is a higher likelihood of shallower water depths. Similarly, as well established in the literature, the distance from the cyclone track can also affect inundation severity (Resio and Westerink, 2008; Jia and Taflanidis, 2013; Contento et al., 2020; Jung et al., 2023; Jung et al., 2024).

In terms of local geographical features, another significant set of factors is associated with adjacent land-use/land-cover features to the POI (Brody et al., 2018; Darabi et al., 2019; Machineni et al., 2019; Mobley et al., 2019; Lin et al., 2023). The overall built environment pattern surrounding a location can be critical in determining its exposure to flooding, as it influences the response of the hydrological system. Large impervious areas (e.g., covered by pavement, roads, rooftops, etc.) reduce surface roughness and infiltration of rainfall into the soil, leading to increased runoff rates and volumes into nearby water bodies. Conversely, pervious surfaces (e.g., riparian areas, green spaces, forest lands, grasslands, etc.) can effectively infiltrate, attenuate, and slowly release water. Green infrastructure (e.g., swales, open spaces, retention ponds and natural wetlands) can also play a determinant role in flood attenuation by storing and holding storm water, thereby mitigating inundation propagation. Moreover, at a smaller spatial scale, the configuration of the urban layout and various local man-made structures can significantly affect inundation propagation mechanisms within a specific area (Testa et al., 2007; Di Baldassarre et al., 2009; Gschnitzer et al., 2017; Bruwier et al., 2020; Mignot and Dewals, 2022; , Bernardini et al., 2021; Di Bacco et al., 2023; Zhu et al., 2023). For instance, levees and embankments, such as those associated with railways or roads, can have a dual effect on flood propagation. While they can act as barriers, preventing inundation from spreading into neighboring areas, they may also redirect floodwaters, thereby potentially increasing the risk of flooding downstream. Their presence can disrupt natural drainage patterns, exacerbating flooding in certain areas. Similarly, bridges may alter flooding mechanisms, restricting downstream water flow and causing water backflow, which may worsen inundation conditions in upstream regions. Additionally, debris accumulation at bridge structures can further impede flow and increase the risk of localized flooding.

Based on this phenomenological analysis, consideration of several features representing potential flooding drivers, including hazard boundary conditions, as well as topological and local geographical characteristics, is necessary for accurately predicting inundation depth

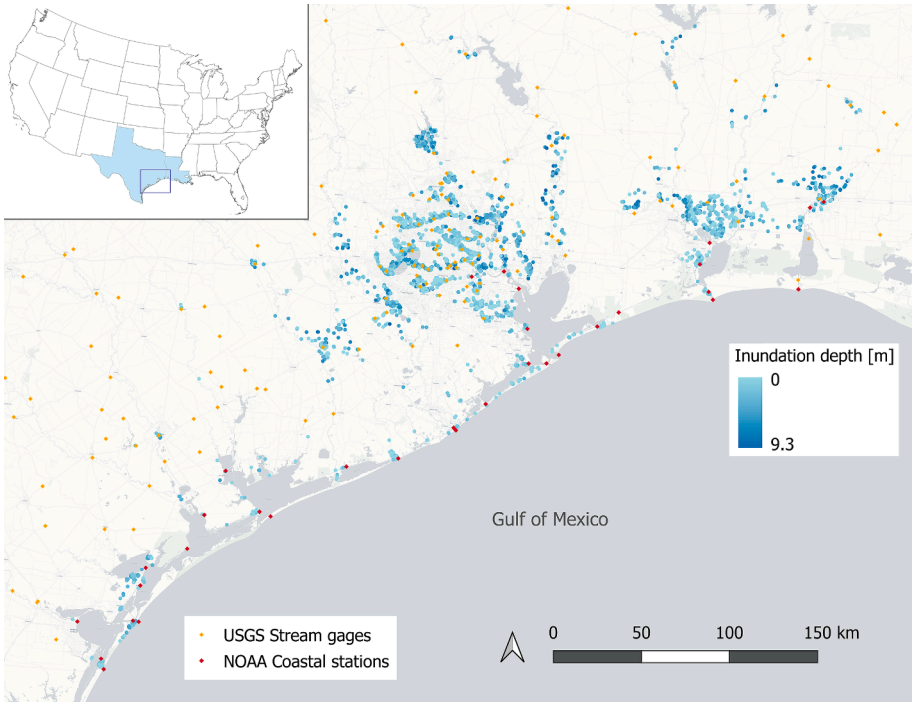

Fig. 3. Overview of the impacted region in Texas and Louisiana (USA) for Hurricane Harvey, with visualization of FEMA inundation depth data considered in the analysis.

within a data-driven approach. While topological and hazard-related features can be straightforwardly assigned to each POI, a more sophisticated approach is required to quantify the influence of spatially distributed geographical features. To this aim, the methodology introduced in Di Bacco et al. (2023) and Scorzini et al. (2024) for tsunamis offers a promising approach, enabling the conversion of distributed areal information into global metrics that incorporate various features influencing inundation at a specific location. The approach employs buffer-related proxies, calculating quantitative indicators to assess the impact of individual features between the POI and the source of hazard, here including the coast (C), the main river network (R), and the cyclone track (T), within predefined buffer areas. The variable related to the i-th proxy with respect to the source of hazard j, with $j = \{C, R, T\}$, is defined as:

$$Pr_{ij} = \frac{I_i}{A_{bj}} \tag{1}$$

where I_i represents either the extent of specific linear or areal features, such as the length of roads or levees, or the area occupied by particular land-uses or building footprints. For point elements, such as bridges, I_i denotes the total number of elements. The denominator, A_b, refers to the buffer area that extends from the POI to the point of minimum distance to the hazard sources. Consequently, Pr_{ij} can be interpreted as the density of the specific feature within each buffer area, allowing for a targeted, physics-informed transfer of two-dimensional information to the POI.

Di Bacco et al. (2023) proposed a buffer geometry represented by irregular hexagons, constructed along the line linking the POI and the nearest point on the coastline. Similarly, for compound flooding, the proposed framework employs analogous buffer polygons connecting the POI with the coastline, the closest element of the main river network, and the cyclone track to account for the influence of the three potential drivers. Fig. 2 illustrates the geometries that can be automatically generated for each individual point in the domain of interest using the source code provided as supplementary material to this manuscript. The width of the buffer geometry is defined as a piecewise linear function of the rectilinear abscissa d which ranges from 0 (at the POI) to D, where D is the distance between the POI and the hazard source. At $d = 0$, the width is the minimum between 100 m and $0.25{\cdot}D$; it increases to $0.5{\cdot}D$ at $d = 0.25{\cdot}D$ and attains a maximum value of $0.6{\cdot}D$ at the hazard source.

2.2. *Machine learning modeling approach for the assessment of the feature importance*

The proposed framework employs a supervised ML model which requires, beyond the aforementioned input features, the knowledge of the response values for a significant number of POIs for effective model training and validation.

Depending on the desired response at POIs, which may be represented by an inundation depth value or a hazard severity class (where inundation depth is ranked into categories according to its damage potential (Scorzini and Leopardi, 2017; Luke et al., 2018; FEMA, 2023), either regression or classification algorithms (Bentivoglio et al., 2022; Karim et al., 2023) can be employed for the assessment of compound flood hazard.

It is worth noting that inundation depth values can be highly sensitive to local irregularities in terrain elevation, such as local depressions, excavations and fills, while absolute water elevation tends to exhibit a smoother spatial distribution (Sebastian et al., 2021). Consequently, this study selects water elevation as the response variable for ML regression models. The inundation depth value is subsequently obtained by subtracting the ground elevation at the POIs, which is not included in the model training process. The resulting hazard severity class is derived from the computed inundation depth, rather than as the response of a ML classification model.

The relevance of the different features for predicting inundation depth is assessed through a backward stepwise model selection process, where the least informative features are progressively discarded. The process starts with a model trained with the entire set of features, which are then ranked using a Permutation Feature Importance (PFI)

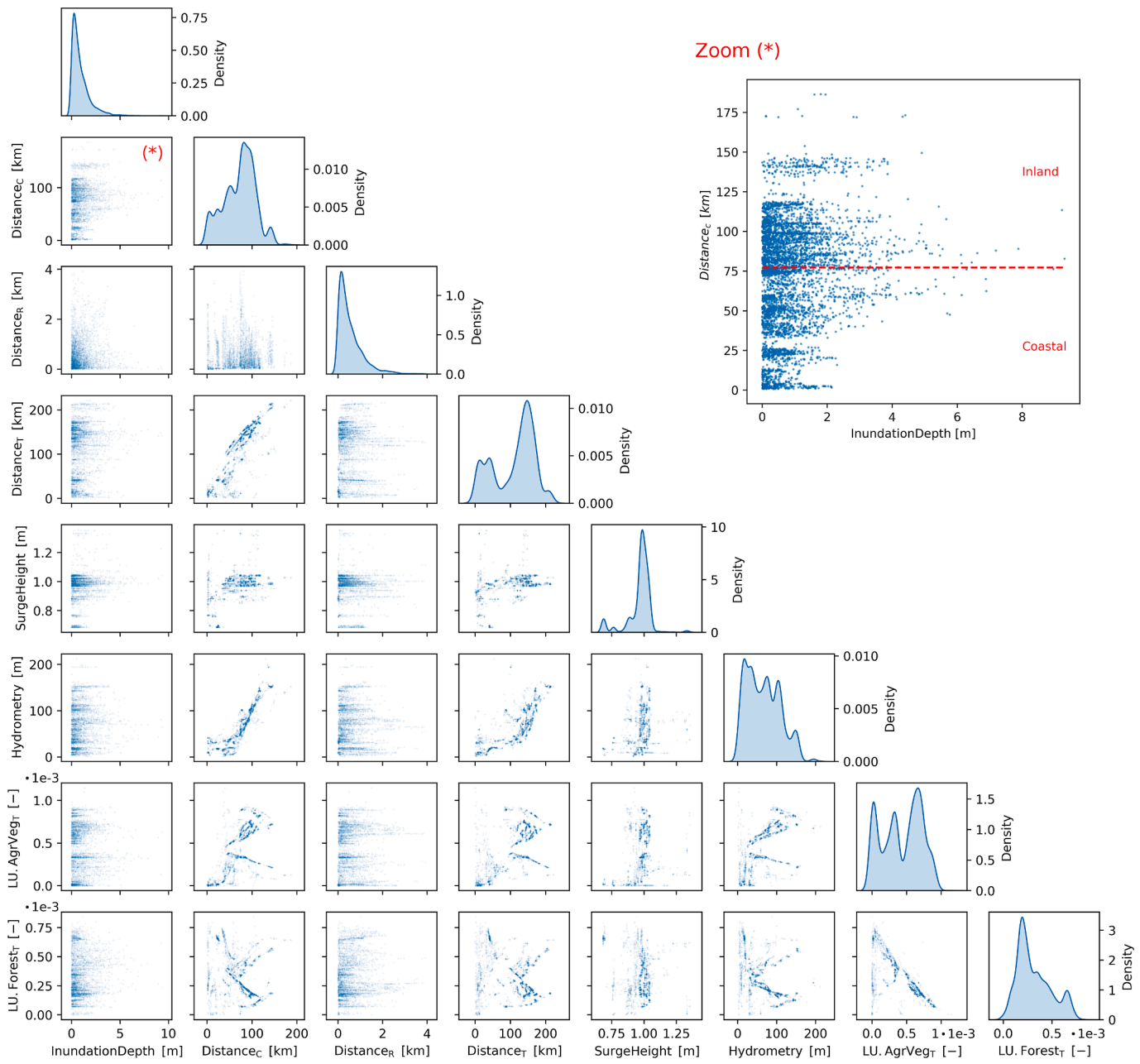

Fig. 4. Pairwise relationships between main hazard, topological and local geographical features across the developed dataset for Hurricane Harvey.

approach. Within the PFI, the rank of each feature is determined by the reduction in prediction accuracy that occurs when the values of the considered feature are shuffled (averaged over multiple repetitions of the shuffling), using a selected error metric as a measure for accuracy (such as the coefficient of determination or the hit rate (HR), respectively, for regression or classification problems).

At each step, the feature with the lowest PFI is removed and the resulting model retrained for the next iteration. Features that provide overlapping information tend to share their importance for the model, which can lead to different PFI rankings as the number of features decreases. Generally, the selection process ends when a significant reduction in accuracy is observed or when a prescribed number of features is reached.

3. Case study: Hurricane Harvey

3.1. Overview of the event

In August 2017, the Houston metropolitan area was struck by Hurricane Harvey. This region experienced an unprecedented amount of rainfall, with accumulations ranging from 900 to 1200 mm over a 5-day period (Van Oldenborgh et al., 2017; Blake and Zelinsky, 2018; Wang et al., 2018). This extreme rainfall, combined with a storm surge ranging from 0.8 to 1.3 m, resulted in catastrophic flooding across numerous areas in Harris and Galveston counties, as well as the broader Houston metropolitan area. Hurricane Harvey stands as a well-documented case study in the literature, owing to the wealth of available meteorological, hydrological, and observed impact data from various sources (including the USGS and FEMA), which makes it suitable to be leveraged in a ML

Table 1
List of considered input features for model development on the Hurricane Harvey case study.

Feature	Feature type	Synthetic description	Data source
Hydrometry	Hazard	Inverse squared distance weighted (ISDW) average of maximum stream gage water levels within a 50 km radius from the point of interest (POI) during the week of hurricane's landfall [m]	Water levels from active stream gages available from the U.S.G.S. National Water Information System (https://waterdata.usgs.gov/nwis). Filtered data for Harvey are also available on HydroShare (USGS & Arctur, 2018)
HydrometryCount		Number of stream gage stations within a 50 km radius from the POI [-]	
HydrometryMinDist		Distance to the nearest stream gage station from the POI [m]	
SurgeHeight		ISDW average of maximum surge heights at NOAA stations during the week of hurricane's landfall, where weights are determined by the squared distances between NOAA stations and the points of minimum distance between the coastline and the POI [m]	Water levels obtained from the Center for Operational Oceanographic Products and Services (CO-OPS) https://tidesandcurrents.noaa.gov/products.html
$Distance_j$	Topological	Minimum distance between the POI and the *j* sources of hazards [m]	Coastline derived from the U.S. Cartographic Boundary Files of the U.S. Census Bureau Track line derived from the International Best Track Archive for Climate Stewardship (IBTrACS) dataset, made available by the World Data Center (WDC) https://www.ncei.noaa.gov/products/international-best-track-archive Nearest element of the main river network derived from the U.S. Geological Survey National Hydrography Dataset (NHDFlowline) https://www.usgs.gov/national-hydrography/national-hydrography-dataset (NHDFlowline has an attribute field name VisibilityFilter which allows for filtering vector data features at eight approximate scales. To identify the main river network for calculating $Distance_R$, only the elements with Visibility > 500,000 were filtered)
Bath100Dist		Minimum distance between the 100 m bathymetric contour and the POI [m]	100 m bathymetric contour derived from the National Centers for Environmental Information (NCEI), Coastal Relief Model (CRM) https://www.ncei.noaa.gov/products/coastal-relief-model
$Buildings_j$	Local geographical (buffer-based)	Building density in buffer *j* (i.e., fraction of the buffer area in the *j*-direction occupied by buildings [m^2/m^2])	Building footprints in Foks et al. (2020)
$Roads_j$		Road density in buffer *j* (i.e., ratio of the total road length to the buffer area in the *j*-direction [m/m^2])	U.S. Census Bureau, Geography Division, TIGER/Line®Shapefiles "Roads" (available in https://catalog.data.gov/dataset)
$Railways_j$		Railway density in buffer *j* (i.e., ratio of the total railway length to the buffer area in the *j*-direction [m/m^2])	U.S. Census Bureau TIGER/Line®Shapefiles "Rails" (available in https://catalog.data.gov/dataset)
$Levees_j$		Levee density in buffer *j* (i.e., ratio of the total levee length to the buffer area in the *j*-direction [m/m^2])	U.S. National Levee Database https://levees.sec.usace.army.mil/
$Bridges_j$		Bridges density in buffer *j* (i.e., ratio of the number of bridges to the buffer area in the *j*-direction [$bridges/m^2$])	U.S. Department of Transportation, U.S. National Bridge Inventory https://geodata.bts.gov/datasets/national-bridge-inventory/
LU. "*type*"$_j$		Fraction of the buffer area in the *j*-direction occupied by a specific land-use type [m^2/m^2] (here, "*type*"=Forest, Desert, Pol&HMon, RockVeg, AgrVeg, SNVeg, OpenWater, OthHumUse)	U.S. Geological Survey Gap Analysis Program, GAP/LANDFIRE National Terrestrial Ecosystems 2011. https://doi.org/10.5066/F7ZS2TM0
$Hydrography_j$		Stream network density in buffer *j* (i.e., ratio of the total length of stream network to the buffer area in the *j*-direction [m/m^2])	U.S. Geological Survey National Hydrography Dataset (NHDFlowline) https://www.usgs.gov/national-hydrography/national-hydrography-dataset
$HydrographyVIS_j$		Visibility-scaled stream network density in buffer *j*, where the total length of river segments within each visibility category is summed and multiplied by the visibility factor before being divided by the buffer area [m/m^2])	
$NaturalWaters_j$		Waterbodies density in buffer *j* (i.e., fraction of the buffer area in the *j*-direction occupied by waterbodies [m^2/m^2])	U.S. Geological Survey National Hydrography Dataset (NHDWaterbodies, such as lakes, ponds, etc.) https://www.usgs.gov/national-hydrography/national-hydrography-dataset To avoid double-counting, original vector layer has been depurated of river-network-type elements

* j = (C,R,T) indicates the three possible directions (coastal, track and river).

approach, complementing the numerous studies in the literature that have primarily examined the event with physically-based hydrologic and hydrodynamic models (Bilskie and Hagen, 2018; Wing et al., 2019; Berens et al., 2021; Valle-Levinson et al., 2020; Chen et al., 2021; Dullo et al., 2021; Huang et al., 2021; Loveland et al., 2021; Sebastian et al., 2021; Li et al., 2022; Maymandi et al., 2022; Schubert et al., 2022; Gutenson et al., 2023; Lee et al., 2023).

3.2. Description of the used dataset

This study leverages inundation depth data sourced from the FEMA Damage Assessment dataset (FEMA, 2023) and designates inundation depth (*InundationDepth*) as response variable. This dataset encompasses information for more than 150,000 locations across the impacted region, covering the metropolitan areas of Houston, Galveston, and Corpus Christi Bay, as well as Sabine and Calcasieu Lakes (Fig. 3). The inundation depth is also categorized by FEMA into four levels, based on their potential damage severity, as follows: (1) 'Affected' (0 m < *InundationDepth* ≤ 0.60 m), (2) 'Minor' (0.60 m < *InundationDepth* ≤ 1.51 m), (3) 'Major' (1.51 m < *InundationDepth* ≤ 2.43 m) and (4) 'Destroyed' (*InundationDepth* > 2.43 m). To optimize both computational efforts (mainly in calculating buffer-related features) and the accuracy and informativeness of results, 5000 data points are randomly sampled from the original FEMA Damage Assessment dataset to form the basis for the present study (Fig. 3). From these watermarks, two subsets are derived based on their distance from the coastline, with the median distance

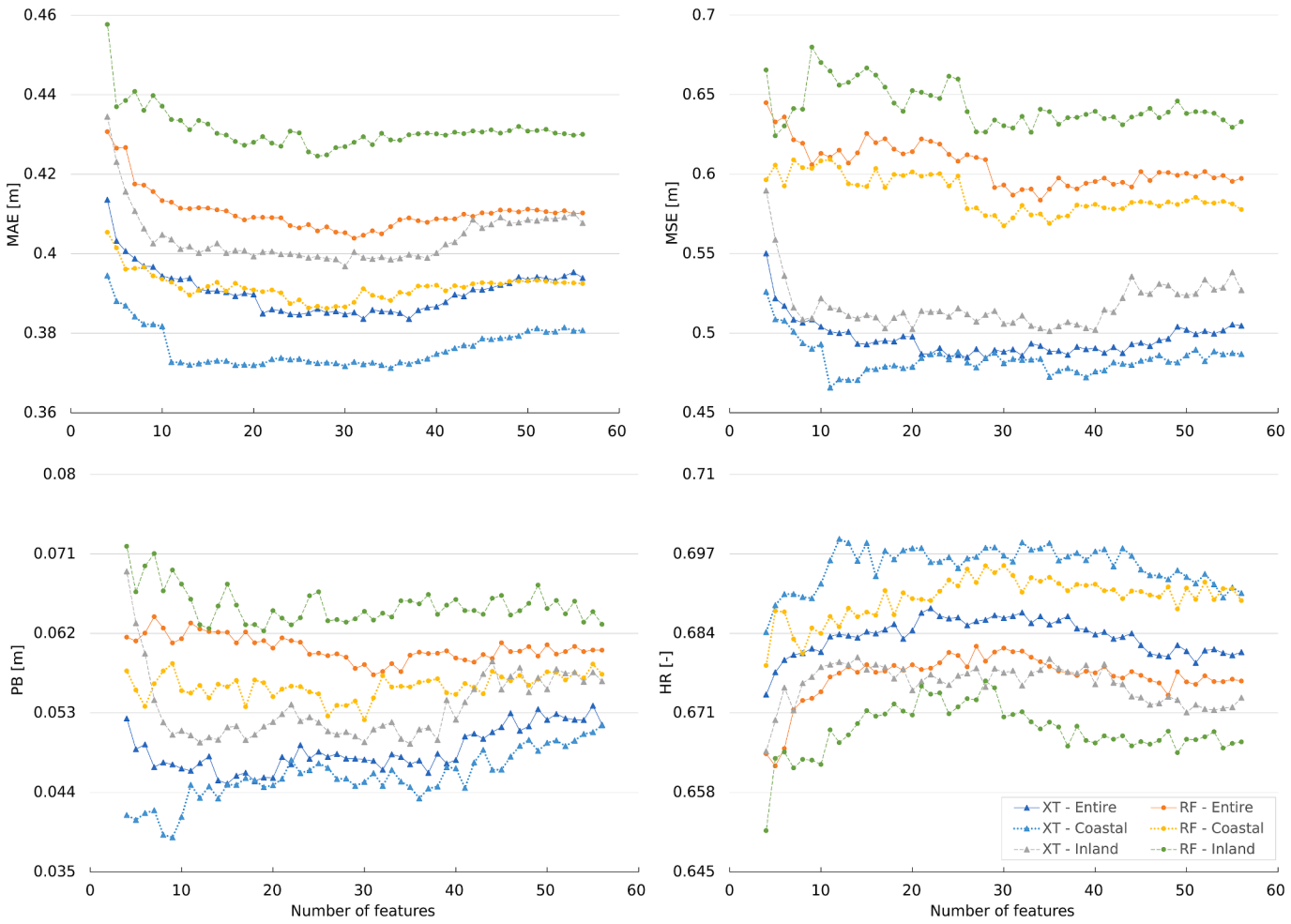

Fig. 5. Evolution of models' (XT and RF) performance across entire, coastal and inland subsets for Hurricane Harvey, with varying number of input features considered in model training.

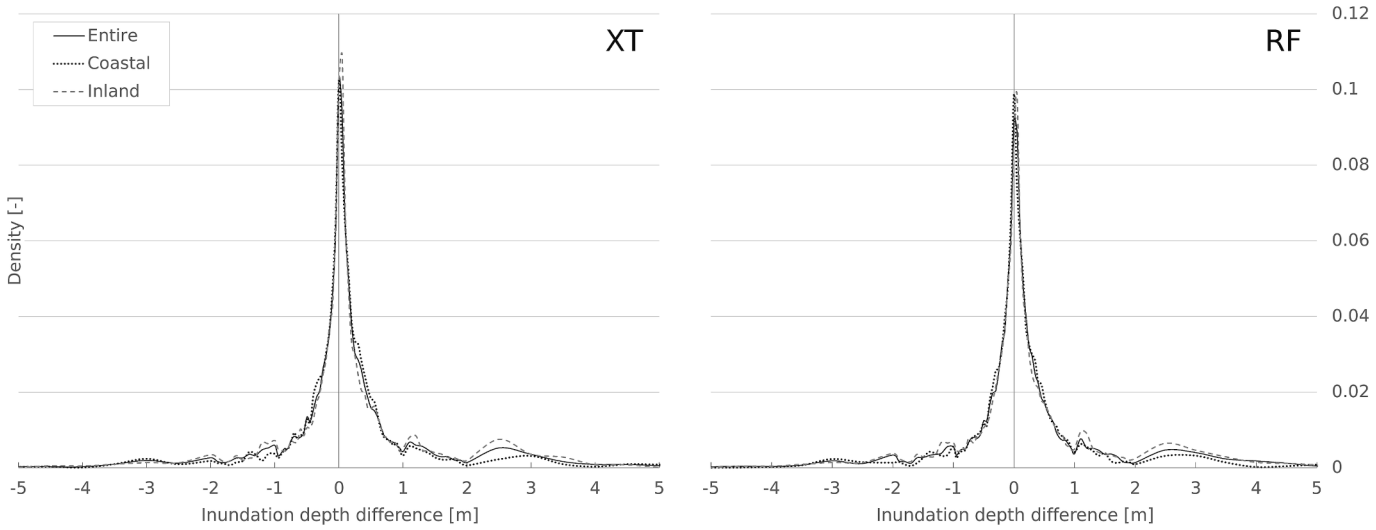

Fig. 6. Distributions of inundation depth difference across entire, coastal and inland subsets for Hurricane Harvey, for models (XT and RF) trained with the 10 most influential features.

value acting as a threshold for distinguishing between the coastal from the inland subset (Fig. 4).

To study the relation between the response variable and its potential drivers, explanatory hazard, topological, and local geographical features' values are assigned to each of the 5000 POI (Table 1). For the input hazard boundary conditions, stream gage water level records from active USGS stations in the impact zone are obtained from the USGS National Water Information System (https://waterdata.usgs.gov/nwis).

The same data, filtered over the Hurricane Harvey event period, is also available in USGS and Arctur (2018) (Fig. 3). From these raw data, the *Hydrometry* feature is calculated by associating to each POI the inverse squared distance weighted (ISDW) average of maximum stream gage water levels within a 50 km radius from the POI during the week of hurricane's landfall. The use of the squared distance as a weighting method for averaging water level data ensures that only meaningful information from the river network is retained, thus minimizing potential bias from unrelated catchments to the POI.

To ensure comprehensiveness, the number of stream gages (*HydrometryCount*) used to calculate *Hydrometry* at each POI, as well as the distance of the nearest stream gage (*HydrometryMinDist*), are also recorded.

Similarly, *SurgeHeight*, serving as the coastal counterpart to *Hydrometry*, is determined for each POI by calculating the ISDW average of maximum surge heights observed at NOAA stations (Fig. 3) during the week of hurricane's landfall. The weights are represented by the squared distances between NOAA stations and the points of minimum distance between the coastline and the POI. Surge heights values at these stations are derived from the Center for Operational Oceanographic Products and Services (CO-OPS). Specifically, water level data and astronomical tide predictions are acquired for the selected stations. The difference between recorded water levels and the astronomical tide predictions provides estimates of surge heights at the NOAA stations.

To determine topological features, basic geospatial operations are used to compute the minimum distances from the POI to hazard origins (i.e., the coastline ($Distance_C$), primary river network ($Distance_R$), and cyclone's track ($Distance_T$)), as well as from the 100 m bathymetric contour (*Bath100Dist*) (Table 1).

To derive features that incorporate local geographical characteristics, for each POI, buffer geometries are generated to represent coastal, river, and track influence areas using the code provided in the Supplementary material. The resulting polygons are used to calculate proxies Pr_{ij} (Eq. (1)). Leveraging available data sources in the region (Table 1), proxies for areal density within each of the three kinds of buffer are derived for structures, infrastructures, and water bodies. The proxies derived for structures and infrastructures include buildings, roads, railways, levees, and bridges (i.e., $Buildings_j$, $Roads_j$, $Railways_j$, $Levees_j$, and $Bridges_j$). Similarly, for water bodies, areal objects such as lakes, ponds, and reservoirs are accounted for through the $NaturalWaters_j$ proxy, while $Hydrography_j$ represents the density of the stream network. The $HydrographyVIS_j$ proxy is introduced to include information on the stream size, as provided in the National Hydrography Dataset with the Visibility filter (Buttenfield et al., 2011).

The same method is used to account for various land-use types characterizing the area of interest, introducing the proxies labeled as $LU.\text{“}type\text{”}_j$ to represent the proportion of each buffer area occupied by a specific land-use type. To achieve this, homogeneous land-use classes from the available land-use layer (Table 1) in the impacted region are aggregated into specific categories defined by “*type*”. The “*type*” distinctions include: *Forest* (Forest & Woodland), *Desert* (Desert & Semi-Desert), *Pol&HMon* (Polar & High Montane Scrub, Grassland & Barrens), *RockVeg* (Open Rock Vegetation), *AgrVeg* (Agricultural & Developed Vegetation), *SNVeg* (Sparse vascular & Nonvascular Rock Vegetation), *OpenWater* (Open Water), and *OthHumUse* (Developed & Other Human Use).

Fig. 4 provides an overview of the final dataset, illustrating kernel densities for some key features and their pairwise relationships; to ensure clarity, amid the 56 considered input features, Fig. 4 focuses on main hazard variables (*Hydrometry*, *SurgeHeight*), topological factors ($Distance_j$), and a subset of representative land-use proxy features ($LU.AgrVeg_T$, $LU.Forest_T$).

3.3. Model development and performance assessment

Instead of conducting an extensive inter-model comparison aimed at identifying the best performing model, which might divert attention from the primary focus of this study, only two ML models have been selected to exemplify the application and effectiveness of the proposed framework using Hurricane Harvey as a case study. Specifically, Extremely Randomized Trees (XT) and Random Forest (RF) (Breiman, 2001; Geurts et al., 2006), are employed within the scikit-learn Python library (Pedregosa et al, 2011).

Both models rely on a bagging procedure to a set of decision trees and are known for their reduced sensibility to overfitting compared to stacking or boosting approaches. For both algorithms, a regression model is developed, with the water elevation as the target response value. Additionally, the obtained values of inundation depth are used to

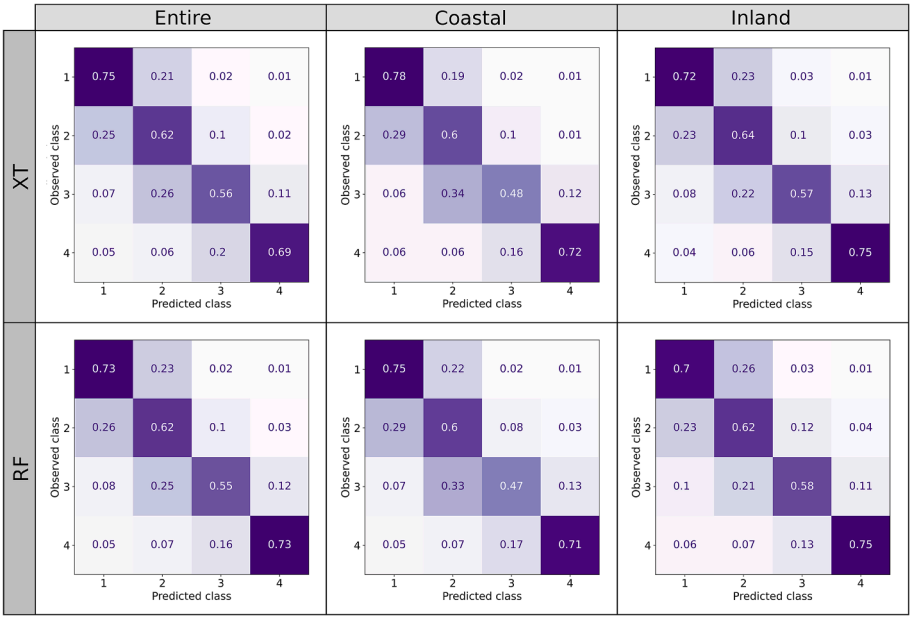

Fig. 7. Row-normalized confusion matrices for XT and RF classifiers trained with the 10 most influential features across entire, coastal and inland subsets for Hurricane Harvey.

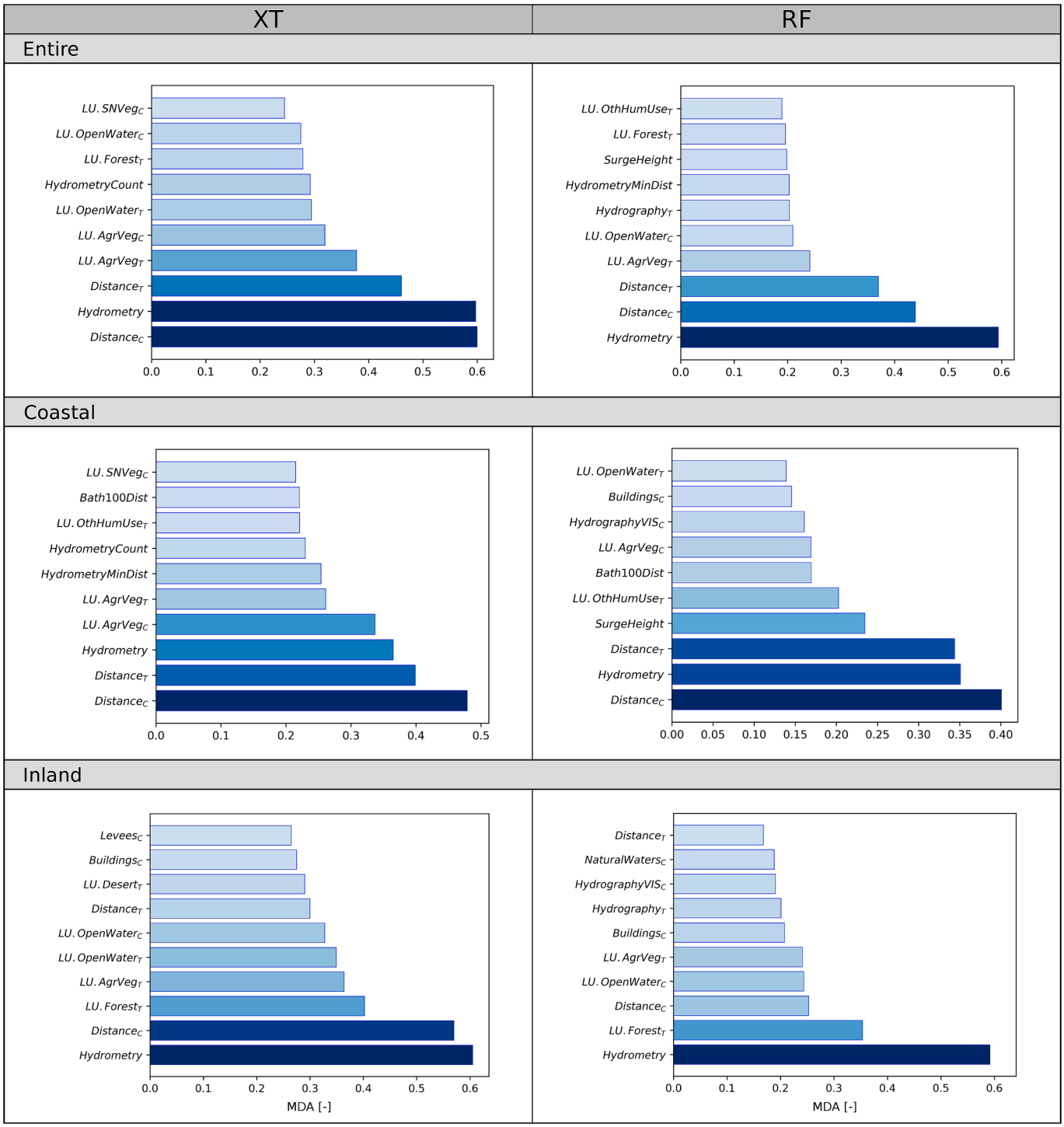

Fig. 8. Analysis of the 10 most important features identified with XT and RF classifiers trained on entire, coastal and inland subsets for Hurricane Harvey. Features are ranked according to their induced mean decrease in accuracy (MDA).

classify the points into the four potential damage severity levels defined by FEMA (as reported in Section 3.2), thereby facilitating an indirect study of a classification problem.

As an initial step in developing XT and RF models, a 5-fold cross-validation with random search is performed to calibrate the hyper-parameters, including the number and maximum depth of the trees, the maximum size of the bootstrap sample used to train each tree, the minimum decrease in impurity, and the minimum samples per leaf. The cross-validation has been chosen to keep all the dataset available for the subsequent phases.

For the second step, which involves model selection as one of the key aspects of this study, the previously mentioned backward selection process is utilized, starting with the initial set of 56 features (Table 1), which are progressively reduced by evaluating their induced mean decrease in the HR as MDA metric. This involves shuffling the values of each feature and averaging the MDA results over 10 repetitions to minimize the impact of random shuffling.

After training the selected regression models, water elevation estimates are obtained from the out-of-bag predictions, i.e. the predictions obtained using each single tree only for the elements not included in the

bootstrap sample used for its training. The predicted inundation depth is then calculated by subtracting the terrain elevation from the predicted water elevation and compared with the observed values. Terrain elevation data are sourced from the pre-event National Elevation Dataset published by USGS (U.S. Geological Survey, 2012), with a resolution of 3 m or 10 m, depending on the spatial coverage over the study area.

For the regression problem, the performance of the models is assessed by computing the Mean Absolute Error (MAE), the Mean Squared Error (MSE), and the Prediction Bias (PB) as per Eqs. 2–4 (Botchkarev, 2019):

$$MAE = \frac{\sum_{i=1}^{n} |\widehat{ID}_i - ID_i|}{n} \tag{2}$$

$$MSE = \frac{\sum_{i=1}^{n} (\widehat{ID}_i - ID_i)^2}{n} \tag{3}$$

$$PB = \frac{\sum_{i=1}^{n} (\widehat{ID}_i - ID_i)}{n} \tag{4}$$

In the equations, $\widehat{ID}_i$ and ID_i denote the predicted and observed values of inundation depth and n is the number of considered watermarks.

For the classification problem, the performance is assessed using the Hit Rate (HR), which is defined as in Eq. (5):

$$HR = \frac{\sum_{i=1}^{4} TP_i}{\sum_{i=1}^{4} (TP_i + FN_i)} \tag{5}$$

where TP_i (True Positives) and FN_i (False Negatives) represent the number of instances correctly classified as class i and the number of instances incorrectly classified as not class i, respectively. Additionally, the row-normalized confusion matrix is examined, with the rows associated to the observed classes and the columns listing the predicted classes; to deal with the class imbalance (50 % of elements in Class 1, 32 % in Class 2, 11 % in Class 3, 7 % in Class 4), the frequencies associated to each matrix element are divided to the number of samples with the corresponding observed class. As a consequence, the main diagonal of the matrix contains the recall of the model over the corresponding inundation depth class.

Models are developed for both the entire dataset of 5000 watermarks and separately for the coastal and inland subsets to analyze potential spatial patterns in the prediction errors and feature importance.

4. Results and discussion

4.1. Feature selection and models' performance

The performance of the XT and RF models for predicting inundation depth is evaluated by systematically reducing the number of features and assessing the models using four error metrics: MAE, MSE, PB for the regression and HR for the classification problem. The results, presented in Fig. 5, clarify the relationship between feature selection and prediction accuracy for the two tested algorithms trained on the entire, coastal, and inland subsets.

When the entire dataset is considered, both models show a decrease in MAE as the number of features approaches 10–20, stabilizing at approximately 0.39 m for the XT and 0.41 m for the RF. The division into the two subsets yields similar results, with MAE reaching about 0.37 m for the coastal subset and 0.40 m for the inland subset. In terms of MSE, the models attain minimum values of about 0.5 m for the XT and 0.6 m for the RF when considering the entire dataset. For the XT model, the coastal subset yields a smaller MSE of about 0.47 m, while the inland predictions exhibit larger minimum MSE values, with the highest being around 0.66 m for the RF. These higher values indicate the greater difficulty the models encounter when predicting inundation depth in inland regions, due to the more complex interplay of factors influencing flood dynamics in such areas, resulting in greater variability in inundation depth. This is evident in the zoomed plot in Fig. 4, where the observed interquartile ranges for inland and coastal regions are respectively equal to 1.08 m and 0.79 m.

Although prediction accuracy is not the main goal of the study but a means to analyze the feature importance, it should be noted that the observed accuracy (Fig. 5) indicates comparable or even superior performance to physics-based models available in existing literature for Hurricane Harvey. For instance, Wing et al. (2019) reported a MAE of about 1 m for estimated water surface elevation at over 1000 water marks in the Hurricane Harvey-impacted region. They used a large-scale flood forecasting product based on the coupling of the Fathom-US hydraulic model with NOAA forecasts of streamflow, rainfall, and surge height. Zheng et al. (2022) validated water levels and inundation extent generated from the National Water Model and the Height Above Nearest Drainage (NWM-HAND) method against observations across the entire Texas impacted domain using 10-m terrain data. They achieved a mean error of −0.39 m over more than 1000 water marks, with further reduction in areas where high-resolution lidar topography was available. Sebastian et al. (2021) utilized the SuperFast INundation of CoastS (SFINCS) hydrodynamic model to analyze flood inundation and damages in Houston. They found a general tendency to overestimation, with a computed MAE of 0.83 m for inundation elevation and 0.36 m for inundation depth based on observed water marks at 115 locations. Li et al. (2022) assessed the performance of CREST-iMAP, a coupled hydrologic-hydraulic model, and reported a mean difference between simulated and observed water depths ranging from 0.51 to 0.60 m, depending on the inclusion of re-infiltration processes into the modeling. Huang et al. (2021) used the Semi-implicit Cross-scale Hydroscience Integrated System Model (SCHISM) to develop a 3D creek-to-ocean model, simulating interactions of major driving factors during Harvey around Galveston Bay, and achieved an overall MAE of 0.65 m calculated over approximately 510 water marks. Similarly, Lee et al. (2023) used the Delft3D Flexible Mesh model to simulate inundation patterns in the Houston-Galveston area, reporting a MAE of 0.62 m in high-resolution coastal areas, which increased to 1.34 m for the entire analyzed region, encompassing 363 water marks. Such comparisons with more complex and computationally demanding models thus demonstrate the potential of data-driven models for efficient prediction of inundation depth during compound flooding events.

With a more in-depth analysis of the results in Fig. 5, the comparison of MSE and MAE values indicates that the predictions include occasional large errors, which are more heavily penalized in the calculation of the MSE. This is further illustrated in Fig. 6, which shows the distributions of inundation depth differences ($\widehat{ID}$– ID) for the three tested subsets using the XT and RF model configurations with the 10 most influential input features. While the majority of the errors clusters in the range ±0.5 m, Fig. 6 also highlights the presence of some larger errors (ranging from ±2 to ±4 m), particularly evident in the inland subset, as reflected in the corresponding error metrics. These error patterns are also evident in the PB (Fig. 5), with minimum values for the entire dataset reaching 0.045 m (with the XT models), as well as in the HR for the classification problem which stabilizes around 0.68 (for both the XT and RF models).

Similar insights can be drawn from a detailed analysis of the results obtained by implementing the XT and RF models to predict inundation depth categories as defined by FEMA (2023). For illustrative purposes, Fig. 7 presents the row-normalized confusion matrices from the application of the XT and RF models trained with the 10 most influential features. These matrices report the classification performance across the entire, coastal and inland subsets, by displaying the observed versus

predicted inundation depth classes. Each cell indicates the portion of instances where a particular observed class is correctly predicted (on the diagonal) or misclassified (all other cells). Fig. 7 reveals that both models perform well in predicting extreme water depth classes (Class 1 and Class 4), but face more difficulties in accurately classifying the intermediate classes (Class 2 and Class 3), consistently across the different subsets. Misclassifications occur more frequently between adjacent classes, as expected due to the gradual transitions in water depth. For the entire dataset, both the XT and RF models show similar performance, with Class 1 and Class 4 being predicted most accurately, resulting in values of HR around 0.74 and 0.72, respectively. The total relative frequency of the elements in the upper diagonal for XT and RF is about 0.15 and 0.16 respectively, with around 0.12 in the lower diagonal for both, globally suggesting a slight overestimation. However, Fig. 7 shows that the samples in Classes 2, 3 and 4 are underestimated on average, with the global result mainly driven by Class 1, accounting for about 50 % of the sample.

Furthermore, Fig. 5 illustrates that the models' performance tends to decline when the number of input features exceeds 40, likely due to overfitting, which occurs when the model captures noise and specific details in the training data that do not generalize well to new, unseen data. Additionally, increasing the number of input features can exponentially expand the feature space, making it more difficult for the model to identify meaningful patterns and thus adding complexity without necessarily enhancing predictive power.

These findings highlight the critical role of feature selection for model development. For the analyzed case, Fig. 5 demonstrates that focusing on the top 10–20 most important features achieves a balance between model complexity and predictive accuracy. More broadly, within a ML framework, similar analyses can guide modelers in tailoring feature selection to the specific characteristics of different regions, thereby optimizing inundation prediction models.

4.2. Analysis of the feature importance

The plot in Fig. 8 illustrates the results of the feature importance analysis performed by using the XT and RF models trained with the top 10 input features, for the entire dataset, as well as the coastal and inland subsets. This part of the analysis is the most clarifying to gain insights into the most relevant features for compound flooding predictions. For this purpose, each subplot of Fig. 8 ranks the features according to their importance in predicting inundation depth class. This ranking is measured by the mean decrease in accuracy (MDA), which reflects the sensitivity of the models' classification accuracy to the input features. A higher value of MDA indicates greater importance attributed to the feature.

Fig. 8 demonstrates that the models exhibit similar trends in feature importance, with some minor differences in the ranking allocations. In particular, for the considered case of Hurricane Harvey, the significance of *Hydrometry* and distance-related features ($Distance_C$ and $Distance_T$) is consistently observed in the top positions, underscoring their critical role for inundation depth prediction. The pairwise relationships among these features, shown in Fig. 4, offer additional insights on their roles. These pair plots reveal non-negligible correlation among the features, but no linear relation with the response variable, *InundationDepth*. This suggests that while they collectively enhance the models' predictive power by capturing similar underlying information and sharing importance, none of them alone can effectively predict inundation depth due to their poor correlation with it.

Region-specific patterns, indicative of the distinct mechanisms governing compound flooding in these areas, are also evident in the list of ancillary features shown in Fig. 8. As expected, coastal flooding is predominantly driven by storm surge and wave action (Lee et al., 2023), which explains the detected importance of *SurgeHeight* in the coastal subset, especially for the RF model. In contrast, inland flooding is more influenced by flood propagation dynamics within the inundated area, where local factors, like density of buildings and water bodies ($Buildings_C$, $LU.OpenWater_{C,T}$), and specific land-use types, play crucial roles. Concerning land-use, types associated with agricultural or vegetated areas (*LU.AgrVeg*, *LU.Forest*) are consistently among the most important features. This aligns with the findings of Yang et al. (2019), who analyzed the relationship between different land-use categories and the occurrence of flooding in the Houston metropolitan area during Hurricane Harvey. Additionally, although the role of coastal forests in mitigating hurricane-induced flooding remains debated in the literature (Resio and Westerink, 2008; Brody et al., 2018; Highfield et al., 2018), the results in Fig. 8 suggest that forested areas played a significant role in inland inundation mechanisms for the specific case analyzed. This is indicated by the proxy $LU.Forest_T$ ranking in the top three features for the inland subset for both XT and RF, and also appearing as important for the entire dataset, albeit in a lower position due to its lesser effect in the coastal region.

The significant importance of *Hydrometry* and distance-related features observed in this study suggests that topographical control played a dominant role in the flooding mechanism during Hurricane Harvey. However, as seen from the results of the model selection process, these features alone do not fully capture the complexities of the inundation process. Other local factors, such as specific land-use types, the presence of water bodies, and man-made structures, influenced flow propagation and retention, affecting fine-scale variations in inundation depth. Differently, river buffer-related features do not appear among the top 10 most important features in any tested subsets (Fig. 8). This can be attributed to the fact that the contributions from fluvial flooding are primarily captured by *Hydrometry*, which provides crucial information on water level rise in the river network, while topological and geographical features in the river direction offer only minor refinements related to inundation propagation characteristics within the floodplain.

It is worth noting that, for the analyzed event, the weights of the ancillary features varied between coastal and inland regions, reflecting the different hydrodynamic conditions and local geographical patterns influencing compound inundation, as also emerged in previous studies (Bilskie and Hagen, 2018; Gori et al., 2020; Mitu et al., 2023). On one hand, this underscores the necessity of considering local-scale territorial specificities for reliable data-driven inundation modeling and, on the other hand, indicates that the relative importance of the driving factors is not generalizable as it is intrinsically tied to the characteristics of the specific examined event.

5. Conclusions

This study presented a machine learning (ML) framework designed to understand the most relevant features needed to predict compound inundation induced by tropical cyclones. The substantial effort required for a ML-based compound flood hazard mapping, in terms of extensive input data retrieval and pre-processing, necessitates an efficient methodology. An a-priori assessment of the relevant features for compound inundation could accelerate the initial steps of model development as well as enhance performance and computational efficiency of the resulting models. However, compound flooding is a complex phenomenon influenced by diverse drivers that vary in importance across and within regions; for this reason, a definitive and unique identification of the most relevant features is neither straightforward nor practical.

The proposed framework, whose applicability has been demonstrated using Hurricane Harvey as a case study, offers a replicable feature selection process for other events and geographical contexts. In particular, the generalizable components of the methodology include the physics-informed identification of explanatory features for compound flooding, the use of a buffer approach for transferring two-dimensional information to the point of interest, and the permutation feature importance method for selecting the most significant features. These elements collectively enhance the model's ability to efficiently predict inundation depths by balancing accuracy and data retrieval

efforts. Nevertheless, the assessment of the specific variables representing the individual drivers of compound flooding must be tailored to the characteristics of each region of implementation, also in consideration of the local availability of data. This tailoring process is probably the more time-consuming aspect of the approach, but it is essential for ensuring the accuracy and reliability of the developed model in diverse geographical contexts.

In this study, the features related to hazard intensity are represented by storm surge and hydrometric levels at coastal and river stations, which inherently incorporate the effects of meteorological and hydrologic drivers to inundation mechanisms. Beyond these hazard features, for Hurricane Harvey, distance metrics resulted of critical importance for accurate predictions, followed by features related to specific land-use types, such as open water and vegetated areas, which help to account for local variability in flooding mechanisms. In this framework, buffer-related proxies, which efficiently condense spatial data into meaningful metrics, proved effective in representing local geographical features. As also observed in the analyzed case, the influence of the various features can vary geographically within the impact area (e.g., coastal and inland areas), thus highlighting the need, for generalizability purposes, to tailor model development and feature selection to specific regional contexts.

It is worth noting that the models presented in this study for Hurricane Harvey do not have any predicting capability for future events because they were calibrated with data from a single storm scenario; however, the proposed framework can be extended to the development of predictive models for future events. Indeed, while unavoidably biased by the consideration of a single storm occurrence, this study demonstrated that the feature importance analysis can effectively reduce the number of variables needed in predictive models for future compound flood events. For this goal, the first step would be to replicate the feature selection process across multiple cyclone scenarios with varying intensities in different regions. A set of control locations (CL) should be identified, ensuring they are as distributed as possible to capture the possible diversity of conditions. Inundation depths from simulations in different scenarios should be sampled at these CLs, and hazard input features related to storm surge levels and river gage data should be provided for the CLs based on the hydraulic conditions at the coastline and along the river network. By being independent of the hazard intensity, the relevant topological and local geographical features identified in this step could be pre-assessed for all points of interest, thus further reducing the computational costs and time of future predictions.

The second phase would involve developing a ML model based on the extended feature importance analysis performed in the first step. The dataset generated initially would be augmented with additional storm scenarios to train the ML model(s), enabling the identification of the relationships between inundation depth and the various features detected previously. To enhance the model's predictive ability, the selection of cyclone events for the training dataset should be as comprehensive as possible, encompassing both historical and extreme synthetic cyclone scenarios that account for future cyclone characteristics projected under a changing climate. Such an approach would ensure more robust and generalizable results, avoiding unreliable extrapolation of predictions beyond the range of the training data.

In this regard, synthetic storms are particularly valuable for regions with limited historical data and are crucial for modeling future scenarios, especially when considering the projected impacts of climate change. However, their selection should be carefully handled, as unrealistic scenarios, with overly regular paths or homogeneous intensity parameters, may not fully capture the complexity of real-world events, potentially introducing an unwanted bias into the inundation model. To avoid overreliance on synthetic scenarios at the expense of historical data, it is essential to strike a balance and integrate both sources to build a robust inundation prediction model. While generating synthetic inundation depth data for model training can be resource- and time-intensive, the availability of large-scale, pre-existing synthetic data from tropical cyclones, such as the US National Storm Surge Risk Maps by NOAA (derived from the simulation of up to 100,000 hypothetical storms across the US using the SLOSH model, (Zachry et al., 2015)) demonstrates that a scalable and generalizable predictive model based on the proposed approach is achievable.

By following the two described steps, the developed ML models can predict spatial inundation patterns within a few seconds, even on a standard commercial laptop, for any future cyclone event with available forecasted storm surge levels (e.g., from NOAA stations) and river gage data (e.g., from USGS stations) at any point within the domain of interest.

CRediT authorship contribution statement

Mario Di Bacco: Writing – review & editing, Visualization, Software, Methodology, Investigation, Formal analysis, Data curation, Conceptualization. **Alessandro Contento:** Writing – review & editing, Investigation, Data curation, Conceptualization. **Anna Rita Scorzini:** Writing – original draft, Visualization, Methodology, Investigation, Data curation, Conceptualization.

Declaration of competing interest

The authors declare that they have no known competing financial interests or personal relationships that could have appeared to influence the work reported in this paper.

Acknowledgments

This work has been partially sponsored by the National Nature Science Foundation of China (NSFC Grant N. W2433120).

Appendix A. Supplementary material

Supplementary data to this article can be found online at https://doi.org/10.1016/j.jhydrol.2024.132262.

Data availability

Data will be made available on request.

References

Abbaszadeh, P., Munoz, D.F., Moftakhari, H., Jafarzadegan, K., Moradkhani, H., 2022. Perspective on uncertainty quantification and reduction in compound flood modeling and forecasting. Iscience 25 (10), 105201. https://doi.org/10.1016/j.isci.2022.105201.

Bentivoglio, R., Isufi, E., Jonkman, S.N., Taormina, R., 2022. Deep learning methods for flood mapping: a review of existing applications and future research directions. Hydrol. Earth Syst. Sci. 26, 4345–4378. https://doi.org/10.5194/hess-26-4345-2022.

Berens, A.S., Palmer, T., Dutton, N.D., Lavery, A., Moore, M., 2021. Using search-constrained inverse distance weight modeling for near real-time riverine flood modeling: Harris County, Texas, USA before, during, and after Hurricane Harvey. Nat. Hazards 105, 277–292. https://doi.org/10.1007/s11069-020-04309-w.

Bernardini, G., Romano, G., Soldini, L., Quagliarini, E., 2021. How urban layout and pedestrian evacuation behaviours can influence flood risk assessment in riverine historic built environments. Sustain. Cities Soc. 70, 102876. https://doi.org/10.1016/j.scs.2021.102876.

Bevacqua, E., Maraun, D., Vousdoukas, M.I., Voukouvalas, E., Vrac, M., Mentaschi, L., Widmann, M., 2019. Higher probability of compound flooding from precipitation and storm surge in Europe under anthropogenic climate change. Sci. Adv. 5 (9), eaaw5531. https://doi.org/10.1126/sciadv.aaw553.

Beven, K., 2012 Rainfall-Runoff Modelling: The Primer. John Wiley & Sons, Ltd. Chichester, West Sussex, UK. 457 pp. ISBN:9781119951001. doi: 10.1002/9781119951001.

Bilskie, M.V., Hagen, S.C., 2018. Defining flood zone transitions in low-gradient coastal regions. Geophys. Res. Lett. 45 (6), 2761–2770. https://doi.org/10.1002/2018GL077524.

Blake, E.S., Zelinsky, D.A., 2018. Tropical cyclone report-Hurricane Harvey (AL092017). National Hurricane Center. Retrieved from https://www.nhc.noaa.gov/data/tcr/AL092017_Harvey.pdf.

Botchkarev, A., 2019. A new typology design of performance metrics to measure errors in machine learning regression algorithms. Interdiscip. J. Inf. Knowl. Manag. 14, 045–076. https://doi.org/10.28945/4184.
Breiman, L., 2001. Random forests. Mach. Learn. 45, 5–32. https://doi.org/10.1023/A:1010933404324.
Brody, S.D., Sebastian, A., Blessing, R., Bedient, P.B., 2018. Case study results from southeast Houston, Texas: identifying the impacts of residential location on flood risk and loss. J. Flood Risk Manage. 11, S110–S120. https://doi.org/10.1111/jfr3.12184.
Bruwier, M., Maravat, C., Mustafa, A., Teller, J., Pirotton, M., Erpicum, S., Archambeau, P., Dewals, B., 2020. Influence of urban forms on surface flow in urban pluvial flooding. J. Hydrol. 582, 124493. https://doi.org/10.1016/j.jhydrol.2019.124493.
Buttenfield, B.P., Stanislawski, L.V., Brewer, C.A., 2011. Adapting generalization tools to physiographic diversity for the United States National Hydrography Dataset. Cartogr. Geogr. Inform. Sci. 38 (3), 289–301. https://doi.org/10.1559/15230406382289.
Camargo, S.J., Wing, A.A., 2021. Increased tropical cyclone risk to coasts. Science 371 (6528), 458–459. https://doi.org/10.1126/science.abg3651.
Chen, M., Li, Z., Gao, S., Luo, X., Wing, O.E., Shen, X., Gourley, J.J., Kolar, R.L., Hong, Y., 2021. A comprehensive flood inundation mapping for Hurricane Harvey using an integrated hydrological and hydraulic model. J. Hydrometeorol. 22 (7), 1713–1726. https://doi.org/10.1175/JHM-D-20-0218.1.
Contento, A., Xu, H., Gardoni, P., 2020. Probabilistic formulation for storm surge predictions. Struct. Infrastruct. Eng. 16 (4), 547–566. https://doi.org/10.1080/15732479.2020.1721543.
Darabi, H., Choubin, B., Rahmati, O., Haghighi, A.T., Pradhan, B., Kløve, B., 2019. Urban flood risk mapping using the GARP and QUEST models: A comparative study of machine learning techniques. J. Hydrol. 569, 142–154. https://doi.org/10.1016/j.jhydrol.2018.12.002.
Di Bacco, M., Rotello, P., Suppasri, A., Scorzini, A.R., 2023. Leveraging data driven approaches for enhanced tsunami damage modelling: Insights from the 2011 Great East Japan event. Environ. Model. Softw. 160, 105604. https://doi.org/10.1016/j.envsoft.2022.105604.
Di Baldassarre, G., Castellarin, A., Brath, A., 2009. Analysis of the effects of levee heightening on flood propagation: example of the River Po, Italy. Hydrol. Sci. J. 54 (6), 1007–1017. https://doi.org/10.1623/hysj.54.6.1007.
Dietrich, J.C., Zijlema, M., Westerink, J.J., Holthuijsen, L.H., Dawson, C., Luettich Jr., R. A., Jensen, R.E., Smith, J.M., Stelling, G.S., Stone, G.W., 2011. Modeling hurricane waves and storm surge using integrally-coupled, scalable computations. Coast. Eng. 58 (1), 45–65. https://doi.org/10.1016/j.coastaleng.2010.08.001.
Dikshit, A., Pradhan, B., Alamri, A.M., 2021. Pathways and challenges of the application of artificial intelligence to geohazards modelling. Gondw. Res. 100, 290–301. https://doi.org/10.1016/j.gr.2020.08.007.
Dullo, T.T., Gangrade, S., Morales-Hernández, M., Sharif, M.B., Kao, S.C., Kalyanapu, A. J., Ghafoor, S., Evans, K.J., 2021. Simulation of Hurricane Harvey flood event through coupled hydrologic-hydraulic models: Challenges and next steps. J. Flood Risk Manage. 14 (3). https://doi.org/10.1111/jfr3.12716.
FEMA (U.S. Federal Emergency Management Administration), 2023. FEMA - Harvey Damage Assessments and Claims. HydroShare. https://doi.org/10.4211/hs.a52d209d46eb42578be0a7472c48e2d5.
Foks, N., Heris, M.P., Bagstad, K.J., Troy, A., 2020. A Code for Rasterizing Microsoft's Building Footprint Dataset. U.S. Geological Survey. doi: 10.5066/P9XZCPMT.
Gao, L., Du, H., Huang, H., Zhang, L., Zhang, P., 2023. Modelling the compound floods upon combined rainfall and storm surge events in a low-lying coastal city. J. Hydrol. 627, 130476. https://doi.org/10.1016/j.jhydrol.2023.130476.
Geurts, P., Ernst, D., Wehenkel, L., 2006. Extremely randomized trees. Mach. Learn. 63, 3–42. https://doi.org/10.1007/s10994-006-6226-1.
Ghanbari, M., Arabi, M., Kao, S.C., Obeysekera, J., Sweet, W., 2021. Climate change and changes in compound coastal-riverine flooding hazard along the US coasts. Earth's. Future 9 (5). https://doi.org/10.1029/2021EF002055.
Gori, A., Lin, N., Xi, D., 2020. Tropical cyclone compound flood hazard assessment: From investigating drivers to quantifying extreme water levels. Earth's. Future 8 (12). https://doi.org/10.1029/2020EF001660.
Gschnitzer, T., Gems, B., Mazzorana, B., Aufleger, M., 2017. Towards a robust assessment of bridge clogging processes in flood risk management. Geomorphology 279, 128–140. https://doi.org/10.1016/j.geomorph.2016.11.002.
Gutenson, J.L., Tavakoly, A.A., Islam, M.S., Wing, O.E., Lehman, W.P., Hamilton, C.O., Wahl, M.D., Massey, T.C., 2023. Comparison of estimated flood exposure and consequences generated by different event-based inland flood inundation maps. Nat. Hazards Earth Syst. Sci. 23 (1), 261–277. https://doi.org/10.5194/nhess-23-261-2023.
Highfield, W.E., Brody, S.D., Shepard, C., 2018. The effects of estuarine wetlands on flood losses associated with storm surge. Ocean Coast. Manag. 157, 50–55. https://doi.org/10.1016/j.ocecoaman.2018.02.017.
Huang, W., Ye, F., Zhang, Y. J., Park, K., Du, J., Moghimi, S., Myers, E., Pe'eri, S., Calzada, J.R., Yu, H.C., Nunez, K. & Liu, Z. (2021). Compounding factors for extreme flooding around Galveston Bay during Hurricane Harvey. Ocean Modelling, 158, 101735. doi: 10.1016/j.ocemod.2020.101735.
IPCC,2023. Summary for Policymakers. In: Climate Change 2023: Synthesis Report. Contribution of Working Groups I, II and III to the Sixth Assessment Report of the Intergovernmental Panel on Climate Change [Core Writing Team, H. Lee and J. Romero (eds.)]. IPCC, Geneva, Switzerland, pp. 1-34, doi: 10.59327/IPCC/AR6-9789291691647.001.
Jia, G., Taflanidis, A.A., 2013. Kriging metamodeling for approximation of high-dimensional wave and surge responses in real-time storm/hurricane risk assessment. Computer Meth. Appl. Mech. Eng. 261, 24–38. https://doi.org/10.1016/j.cma.2013.03.012.
Jung, W.H., Taflanidis, A.A., Kyprioti, A.P., Adeli, E., Westerink, J.J., Tolman, H., 2023. Efficient probabilistic storm surge estimation through adaptive importance sampling across storm advisories. Coast. Eng. 183, 104287. https://doi.org/10.1016/J.COASTALENG.2023.104287.
Jung, W.H., Taflanidis, A.A., Nadal-Caraballo, N.C., Yawn, M.C., Aucoin, L.A., 2024. Regional storm surge hazard quantification using Gaussian process metamodeling techniques. Nat. Hazards 120, 755–783. https://doi.org/10.1007/s11069-023-06195-4.
Karim, F., Armin, M.A., Ahmedt-Aristizabal, D., Tychsen-Smith, L., Petersson, L., 2023. A review of hydrodynamic and machine learning approaches for flood inundation modeling. Water 15 (3), 566. https://doi.org/10.3390/w15030566.
Kohno, N., Dube, S.K., Entel, M., Fakhruddin, S.H.M., Greenslade, D., Leroux, M.D., Rhome, J., Thuy, N.B., 2018. Recent progress in storm surge forecasting. Trop. Cyclone Res. Rev. 7 (2), 128–139. https://doi.org/10.6057/2018TCRR02.04.
Lee, W., Sun, A.Y., Scanlon, B.R., Dawson, C., 2023. Hindcasting compound pluvial, fluvial and coastal flooding during Hurricane Harvey (2017) using Delft3D-FM. Nat. Hazards 120, 851–880. https://doi.org/10.1007/s11069-023-06247-9.
Li, Z., Chen, M., Gao, S., Wen, Y., Gourley, J.J., Yang, T., Kolar, R., Hong, Y., 2022. Can re-infiltration process be ignored for flood inundation mapping and prediction during extreme storms? A case study in Texas Gulf Coast region. Environ. Model. Softw. 155, 105450. https://doi.org/10.1016/j.envsoft.2022.105450.
Lin, N., Emanuel, K., Oppenheimer, M., Vanmarcke, E., 2012. Physically based assessment of hurricane surge threat under climate change. Nat. Clim. Chang. 2 (6), 462–467. https://doi.org/10.1038/nclimate1389.
Lin, J., Zhang, W., Wen, Y., Qiu, S., 2023. Evaluating the association between morphological characteristics of urban land and pluvial floods using machine learning methods. Sustain. Cities Soc. 99, 104891. https://doi.org/10.1016/j.scs.2023.104891.
Loveland, M., Kiaghadi, A., Dawson, C.N., Rifai, H.S., Misra, S., Mosser, H., Parola, A., 2021. Developing a modeling framework to simulate compound flooding: when storm surge interacts with riverine flow. Front. Clim. 2, 609610. https://doi.org/10.3389/fclim.2020.609610.
Luke, A., Sanders, B.F., Goodrich, K.A., Feldman, D.L., Boudreau, D., Eguiarte, A., Serrano, K., Reyes, A., Schubert, J.E., AghaKouchak, A., Basolo, V., Matthew, R.A., 2018. Going beyond the flood insurance rate map: Insights from flood hazard map co-production. Nat. Hazards Earth Syst. Sci. 18 (4), 1097–1120. https://doi.org/10.5194/nhess-18-1097-2018.
Machineni, N., Sinha, V.S., Singh, P., Reddy, N.T., 2019. The impact of distributed landuse information in hydrodynamic model application in storm surge inundation. Estuar. Coast. Shelf Sci. 231, 106466. https://doi.org/10.1016/j.ecss.2019.106466.
Marsooli, R., Lin, N., Emanuel, K., Feng, K., 2019. Climate change exacerbates hurricane flood hazards along US Atlantic and Gulf Coasts in spatially varying patterns. Nat. Commun. 10 (1), 3785. https://doi.org/10.1038/s41467-019-11755-z.
Maymandi, N., Hummel, M.A., Zhang, Y., 2022. Compound coastal, fluvial, and pluvial flooding during historical hurricane events in the Sabine-Neches Estuary, Texas. Water Resources Res. 58 (12). https://doi.org/10.1029/2022WR033144.
Mignot, E., Dewals, B., 2022. Hydraulic modelling of inland urban flooding: Recent advances. J. Hydrol. 609, 127763. https://doi.org/10.1016/j.jhydrol.2022.127763.
Mitu, M.F., Sofia, G., Shen, X., Anagnostou, E.N., 2023. Assessing the compound flood risk in coastal areas: Framework formulation and demonstration. J. Hydrol. 626, 130278. https://doi.org/10.1016/j.jhydrol.2023.130278.
Mobley, W., Sebastian, A., Highfield, W., Brody, S.D., 2019. Estimating flood extent during Hurricane Harvey using maximum entropy to build a hazard distribution model. J. Flood Risk Manage. 12. https://doi.org/10.1111/jfr3.12549.
Moftakhari, H., Schubert, J.E., AghaKouchak, A., Matthew, R.A., Sanders, B.F., 2019. Linking statistical and hydrodynamic modeling for compound flood hazard assessment in tidal channels and estuaries. Adv. Water Resour. 128, 28–38. https://doi.org/10.1016/j.advwatres.2019.04.009.
Moradian, S., AghaKouchak, A., Gharbia, S., Broderick, C., Olbert, A.I., 2024. Forecasting of compound ocean-fluvial floods using machine learning. J. Environ. Manage. 364, 121295. https://doi.org/10.1016/j.jenvman.2024.121295.
Pedregosa, F., Varoquaux, G., Gramfort, A., Michel, V., Thirion, B., Grisel, O., Duchesnay, É., 2011. Scikit-learn: Machine learning in Python. J. Mach. Learn. Res. 12, 2825–2830.
Peel, M.C., McMahon, T.A., 2020. Historical development of rainfall-runoff modeling. Wiley Interdiscip. Rev. Water 7 (5). https://doi.org/10.1002/wat2.1471.
Resio, D.T., Westerink, J.J., 2008. Modeling the physics of storm surges. Phys. Today 61 (9), 33–38. https://doi.org/10.1063/1.2982120.
Saksena, S., Dey, S., Merwade, V., Singhofen, P.J., 2020. A computationally efficient and physically based approach for urban flood modeling using a flexible spatiotemporal structure. Water Resour. Res. 56 (1). https://doi.org/10.1029/2019WR025769.
Santiago-Collazo, F.L., Bilskie, M.V., Hagen, S.C., 2019. A comprehensive review of compound inundation models in low-gradient coastal watersheds. Environ. Model. Softw. 119, 166–181. https://doi.org/10.1016/j.envsoft.2019.06.002.
Schubert, J.E., Luke, A., AghaKouchak, A., Sanders, B.F., 2022. A framework for mechanistic flood inundation forecasting at the metropolitan scale. Water Resour. Res. 58 (10). https://doi.org/10.1029/2021WR031279.
Scorzini, A.R., Leopardi, M., 2017. River basin planning: From qualitative to quantitative flood risk assessment: The case of Abruzzo Region (central Italy). Nat. Hazards 88, 71–93. https://doi.org/10.1007/s11069-017-2857-8.
Scorzini, A.R., Di Bacco, M., Sugawara, D., Suppasri, A., 2024. Machine learning and hydrodynamic proxies for enhanced rapid tsunami vulnerability assessment. Commun. Earth Environ. 5 (1), 301. https://doi.org/10.1038/s43247-024-01468-7.

Sebastian, A., Bader, D.J., Nederhoff, C.M., Leijnse, T.W.B., Bricker, J.D., Aarninkhof, S. G.J., 2021. Hindcast of pluvial, fluvial, and coastal flood damage in Houston, Texas during Hurricane Harvey (2017) using SFINCS. Nat. Hazards 109, 2343–2362. https://doi.org/10.1007/s11069-021-04922-3.

Tanim, A.H., Goharian, E., 2021. Developing a hybrid modeling and multivariate analysis framework for storm surge and runoff interactions in urban coastal flooding. J. Hydrol. 595, 125670. https://doi.org/10.1016/j.jhydrol.2020.125670.

Tanim, A.H., McKinnie, F.W., Goharian, E., 2024. Coastal Compound Flood Simulation through Coupled Multidimensional Modeling Framework. J. Hydrol. 630, 130691. https://doi.org/10.1016/j.jhydrol.2024.130691.

Testa, G., Zuccala, D., Alcrudo, F., Mulet, J., Soares-Frazão, S., 2007. Flash flood flow experiment in a simplified urban district. J. Hydraul. Res. 45 (sup1), 37–44. https://doi.org/10.1080/00221686.2007.9521831.

U.S. Geological Survey (2012). National Elevation Dataset, accessed October 23 at URL https://www.sciencebase.gov/catalog/item/4fcf8fd4e4b0c7fe80e81504.

USGS & Arctur, 2018. Harvey Gaged Streamflow Timeseries. HydroShare. https://doi.org/10.4211/hs.51d1539bf6e94b15ac33f7631228118c.

Valle-Levinson, A., Olabarrieta, M., Heilman, L., 2020. Compound flooding in Houston-Galveston bay during Hurricane Harvey. Sci. Total Environ. 747, 141272. https://doi.org/10.1016/j.scitotenv.2020.141272.

Van Oldenborgh, G.J., Van Der Wiel, K., Sebastian, A., Singh, R., Arrighi, J., Otto, F., Haustein, K., Li, S., Vecchi, G., Cullen, H., 2017. Attribution of extreme rainfall from Hurricane Harvey, August 2017. Environ. Res. Lett. 12 (12), 124009. https://doi.org/10.1088/1748-9326/aa9ef2.

Wahl, T., Jain, S., Bender, J., Meyers, S.D., Luther, M.E., 2015. Increasing risk of compound flooding from storm surge and rainfall for major US cities. Nat. Clim. Chang. 5 (12), 1093–1097. https://doi.org/10.1038/nclimate2736.

Wang, S.S., Zhao, L., Yoon, J.H., Klotzbach, P., Gillies, R.R., 2018. Quantitative attribution of climate effects on Hurricane Harvey's extreme rainfall in Texas. Environ. Res. Lett. 13 (5), 054014. https://doi.org/10.1088/1748-9326/aabb85.

Wing, O.E., Sampson, C.C., Bates, P.D., Quinn, N., Smith, A.M., Neal, J.C., 2019. A flood inundation forecast of Hurricane Harvey using a continental-scale 2D hydrodynamic model. J. Hydrol. X 4, 100039. https://doi.org/10.1016/j.hydroa.2019.100039.

Xu, K., Wang, C., Bin, L., 2023. Compound flood models in coastal areas: a review of methods and uncertainty analysis. Nat. Hazards 116 (1), 469–496. https://doi.org/10.1007/s11069-022-05683-3.

Yang, D., Yang, A., Qiu, H., Zhou, Y., Herrero, H., Fu, C.S., Yu, Q., Tang, J., 2019. A citizen-contributed GIS approach for evaluating the impacts of land use on hurricane-Harvey-induced flooding in Houston area. Land 8 (2), 25. https://doi.org/10.3390/land8020025.

Zachry, B.C., Booth, W.J., Rhome, J.R., Sharon, T.M., 2015. A national view of storm surge risk and inundation. Weather Clim. Soc. 7 (2), 109–117. https://doi.org/10.1175/WCAS-D-14-00049.1.

Zahura, F.T., Goodall, J.L., 2022. Predicting combined tidal and pluvial flood inundation using a machine learning surrogate model. J. Hydrol.: Reg. Stud. 41, 101087. https://doi.org/10.1016/j.ejrh.2022.101087.

Zheng, X., D'Angelo, C., Maidment, D.R., Passalacqua, P., 2022. Application of a Large-Scale Terrain-Analysis-Based Flood Mapping System to Hurricane Harvey. JAWRA J. Am. Water Resour. Assoc. 58 (2), 149–163. https://doi.org/10.1111/1752-1688.12987.

Zhong, M., Xiao, L., Li, X., Mei, Y., Jiang, T., Song, L., Chen, X., 2024. A study on compound flood prediction and inundation simulation under future scenarios in a coastal city. J. Hydrol. 628, 130475. https://doi.org/10.1016/j.jhydrol.2023.130475.

Zhu, Z., Gou, L., Liu, S., Peng, D., 2023. Effect of urban neighbourhood layout on the flood intrusion rate of residential buildings and associated risk for pedestrians. Sustain. Cities Soc. 92, 104485. https://doi.org/10.1016/j.scs.2023.104485.

Zscheischler, J., Westra, S., Van Den Hurk, B.J., Seneviratne, S.I., Ward, P.J., Pitman, A., AghaKouchak, A., Bresch, D.N., Leonard, M., Wahl, T., Zhang, X., 2018. Future climate risk from compound events. Nat. Clim. Chang. 8 (6), 469–477. https://doi.org/10.1038/s41558-018-0156-3.